ACS APPLIED MATERIALS & INTERFACES

Surfaces, Interfaces, and Applications

Application of Antibody-Powered Triplex-DNA Nanomachine to Electrochemiluminescence Biosensor for Detection of Anti-Digoxigenin with Improved Sensitivity versus Cycling Strand Displacement Reaction

Shan-Shan Yang, Ming-Hui Jiang, Yaqin Chai, Ruo Yuan, and Ying Zhuo

ACS Appl. Mater. Interfaces, **Just Accepted Manuscript** • DOI: 10.1021/acsami.8b16157 • Publication Date (Web): 11 Oct 2018

ACS Publications

is published by the American Chemical Society. 1155 Sixteenth Street N.W., Washington, DC 20036

Application of Antibody-Powered Triplex-DNA Nanomachine to Electrochemiluminescence Biosensor for Detection of Anti-Digoxigenin with Improved Sensitivity versus Cycling Strand Displacement Reaction

Shan-Shan Yang, Ming-Hui Jiang, Ya-Qin Chai, Ruo Yuan*, and Ying Zhuo*

Key Laboratory of Luminescent and Real-Time Analytical Chemistry (Southwest University), Ministry of Education, College of Chemistry and Chemical Engineering, Southwest University, Chongqing 400715, PR China

KEYWORDS: triplex-DNA; electrochemiluminescence; rubrene microblocks; anti-digoxigenin; porous palladium nanospheres; co-reaction accelerator

* Corresponding author. **Tel:** +86-23-68252277; **Fax:** +86-23-68253172.

E-mail address: yuanruo@swu.edu.cn (R. Yuan), yingzhuo@swu.edu.cn. (Y. Zhuo).

ABSTRACT

The accurate and rapid quantitative detection of antibodies had a significant influence in controlling and preventing diseases or toxins outbreaks. In this work, we first introduce the antibody-powered triplex-DNA nanomachine to release cargo DNA as substitute target for sensitive electrochemiluminescence (ECL) detection of anti-digoxigenin based on a novel ternary ECL system. It is worth noting that the cargo DNA as a substitute target of antibody can further participate in an enzyme-assisted cycling strand displacement reaction (CSDR) to achieve ECL signal amplification and improve the sensitivity of antibody detection. Additionally, porous palladium nanospheres (pPdNSs) with considerably catalytic activity were first applied as co-reaction accelerator to efficiently enhance the intensity of the ECL system of rubrene microblocks (RubMBs) as luminophore and dissolved O_2 as endogenous co-reactant. With the resultant ternary ECL system as biosensing platform, a significantly enhanced initial signal was achieved in advance. Then the ferrocene labeled quenching probes were employed to reduce initial signal and obtain the low background signal. Eventually, the cargo DNA made the quenching probes release and recover the signal in the presence of anti-digoxigenin. Thereupon the wide linear range (0.01-200 nM) and low limit of detection (6.7 pM) were obtained, and this method not only reduces conjugation steps, but also provides a sensitive and novel ECL analysis platform for trace detection of other antibodies and antigen.

1. Introduction

Special antibody detection[1-3] has served as one of the most important means of clinical diagnosis, due to its significant role in controlling and preventing diseases or toxins outbreaks.[4] To date, besides the traditional enzyme-linked immunosorbent assays[5] and immunoblotting methods[6], some novel strategies in optical and electrochemical methods[7-9] for antibody detection have emerged in recent years. For example, Alexis et al.[10] proposed an electrochemical steric-hindrance approach for effective detection of antibody based on the hindrance effect of immunocomplex towards the electronic transmission of redox signal probes. Additionally, Zhang and co-workers[11] introduced an optical binding assays for antibody detection based on strand displacement competition reaction according to biotin-streptavidin interaction and Förster resonance energy transfer (FRET) signal strategy. However, the lack of amplification methods for the direct detection of antibody limits its sensitivity improvement, which makes the detection of trace antibodies highly challenging. Recently, target conversion strategy creates a desirable opportunity for target amplification according to the conversion of targets into nucleic acids which serve as ideal amplifiable "substitute target" for any non-nucleic acid targets. Generally, the targets, such as proteins and small biomolecules, are converted into aptamer-protein complex, and further participated in nucleic acid recycling amplification to achieve sensitive detection of non-nucleic acid targets.[12,13] Nevertheless,

the aptamers with high specificity and affinity were involved in the conversion of aptamer-target complex into nucleic acids, which depended on the aptamers obtained by the laborious and costly selection. To avoid the dependence of aptamer, our previous work[14] has introduced a target conversion strategy by the use of DNA-antibody binding complex and nucleic acid amplification for electrochemical detection of Cystatin C. However, this method required multiple, time-consuming conjugation steps. Herein, we describes a relatively simply, time-saving method for antibody detection, which combines triplex-DNA nanomachine for target conversion with enzyme-assisted cycling strand displacement reaction (CSDR) for signal amplification.

Electrochemiluminescence (ECL) with high sensitivity[15-17] is considered as an effective analytical technology[18], for the detection and quantization of low abundance analytes[19]. With the advantages of high fluorescence quantum efficiency and low cost, organic ECL luminophores, such as rubrene[20], 9,10-diphenylanthracene (DPA)[21] and boron dipyrromethene (BODIPY)[22] have been studied extensively in the past few decades. However, handicapping by their nature aromatic structure, the most organic ECL luminophores demonstrate weak ECL signal in aqueous solution due to the poor solubility and low radical ion stability, which limits their applications in bioanalysis. Until 2014, Bard and co-workers[23] first reported the ECL of rubrene in emulsion system in water. As described, it not only increased the solubility of rubrene in water in a sense, but enhanced the ECL intensity by using tri-n-propylamine (TPrA) as the exogenous

co-reactant as well. And yet, both the weak stability of emulsion and the security of the used reagents are obvious issues of this method. Recently, in our previous reports[24], the strong ECL of rubrene microrods (RubMRs) prepared by reprecipitation method was first achieved just in phosphate-buffered saline (dissolved O_2 as endogenous co-reactant) with the enhancement of Pt nanoflowers (PtNFs). Different from this, we proposed a solid phase ternary ECL system with porous palladium nanospheres (abbreviated as pPdNSs and played the role as co-reaction accelerator) assembled RubMBs as enhanced luminophores and dissolved O_2 as endogenous co-reactant. Advantages of the proposed ECL system can be summarized as the following. First, pPdNSs can extremely increase the ECL signal of the RubMBs/dissolved O_2 system about 3 times as much as that of PtNFs. Secondly, palladium as non-toxic noble metal is cheaper and more economical than platinum, and the synthesis method of pPdNSs is simple and time-saving. Besides, the RubMBs with uniform size were synthesized by the usage of the tween 20 as surfactant, which can maintain original morphology in aqueous phase for a long time. All of these advantages ameliorate greatly the ECL performance of the RubMBs/dissolved O_2 ECL system.

Here we first introduced the target-powered triplex-DNA nanomachine[25,26] into the ternary ECL system (RubMBs/dissolved O_2/pPdNSs) and utilized enzyme-assisted CSDR to achieve highly sensitive and specific detection of target anti-digoxigenin (anti-Dig). In our work, the triplex-DNA nanomachine was labeled on Au nanoparticles decorated

Fe_3O_4 magnetic nanoparticles (triplex-DNA/Au@Fe_3O_4 composites), and then reacted with different concentrations of target anti-Dig to release the cargo DNA as amplifiable substitute target, which further participates in enzyme-assisted CSDR to achieve ECL signal amplification and improve the sensitivity for anti-Dig detection. Subsequently, we constructed the following ECL sensing platform. Briefly, RubMBs and pPdNSs were assembled onto the GCE by electrostatic interaction, respectively, which presented the "signal on" state. Importantly, not only had the pPdNSs with porous nanostructures considerably catalytic activity for the RubMBs/dissolved O_2 ECL system, but provided numerous sites for thiol-labeled DNA probe immobilization as well. Then, the S4-S5-Fc duplex as quenching probe was assembled on pPdNSs *via* Pd-S bond to reduce the background signal enormously, which exhibited the "signal off" state. Finally, the substitute target with different concentrations was incubated on the surface of modified electrode, and then triggered the CSDR with the aid of the T7 Exonuclease (T7 Exo). As expected, it was observed that the ECL signal realized partial recovery as the "signal on" state. Meanwhile, it can be found that the ECL intensity increased with the increasing concentration of target anti-Dig. Therefore, the proposed biosensor can be successfully applied for anti-Dig sensitive detection with brilliant selectivity, satisfactory stability and low limit of detection. This method not only reduces conjugation steps, but also achieves sensitive detection of antibody. The construction process of the biosensor is shown in Scheme 1.

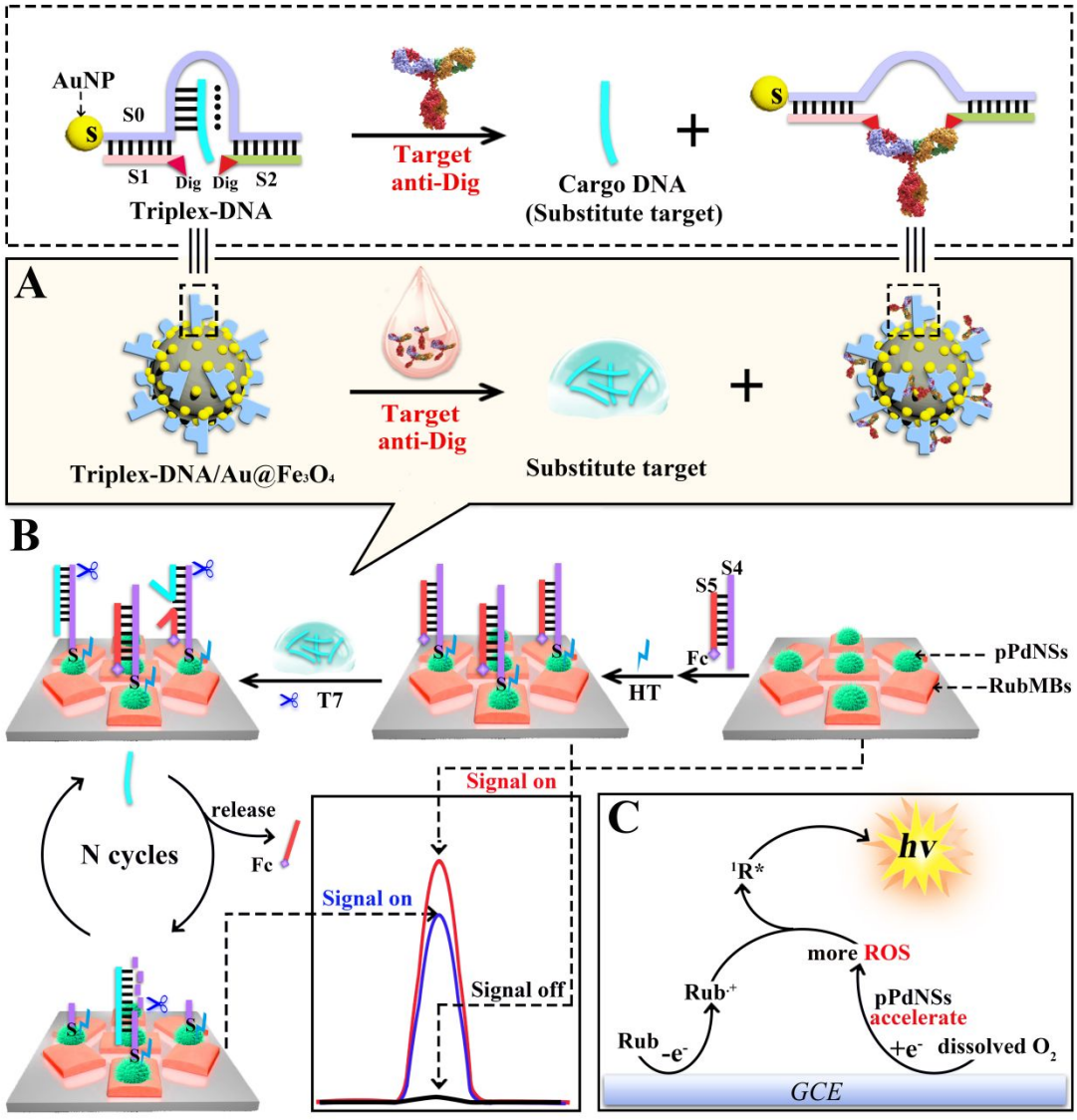

Scheme 1. Schematic illustration of production process of substitute target (A), Sensitive detection of anti-Dig based on enzyme-assisted cycling strand displacement reaction (B), and the possible ECL mechanism of ternary RubMBs/dissolved O_2/pPdNSs system (C).

2. Experimental methods

2.1 Preparation of $Au@Fe_3O_4$ nanocomposites

The $Au@Fe_3O_4$ nanocomposites were synthesized according to the published

method with slightly alterations.[27,28] Firstly, 0.35 g ferric chloride ($FeCl_3 \cdot 6H_2O$), 0.25 g polyethylene glycol-800 (PEG-800) and 0.9 g natrium aceticum (NaAc) were dissolved into 10 mL ethylene glycol under moderately stirring for 30 min. Secondly, the resultant solution was poured into a 20 mL stainless-steel autoclave and reacted at 200 ºC for 8 h. After terminating the reaction and cooling down to room temperature, the black Fe_3O_4 precipitate was collected *via* magnetic separation and washed alternately using ethanol (95%) and ultrapure water for four times. Subsequently, the obtained Fe_3O_4 magnetic nanomaterials were dried overnight at 80 ºC. Then, 10 mg as-prepared Fe_3O_4 nanomaterials were dispersed in 10 mL poly-(diallyldimethylammonium chloride) (PDDA) solution (1%). Next, the above mixture was shaken overnight under room temperature, and then centrifugated to remove the unnecessary PDDA. Following this, 2 mL the gold colloidal solution prepared by an as-reported method[29] was injected into the above PDDA-functionalized Fe_3O_4 solution, and then shook for 4 h under room temperature to form the Au@Fe_3O_4 nanocomposites. Then the products were separated by a magnet and washed four times using ultrapure water. Eventually the as-prepared Au@Fe_3O_4 nanocomposites were dispersed in 8 mL ultrapure water and stored at 4 ºC for the next experiment. The scanning electron microscope (SEM) image of Au@Fe_3O_4 nanocomposites was presented in Figure S1 (Supporting Information).

2.2 Synthesis of rubrene microblocks and porous palladium nanospheres

The rubrene microblocks (RubMBs) were synthetized through a typical

reprecipitation method as follows. Briefly, 10 mg orange rubrene powder was dispersed in 10 mL tetrahydrofuran (THF) with vigorous stirring, followed by being injected into 5 mL tween 20 (0.24 g/mL) aqueous solution under rapid agitation for 10 min. Subsequently, the mixture was ultrasonicated for 30 min. Thereafter, the RubMBs were collected through centrifugation and washed five times using ultrapure water to remove residual THF and tween 20. Finally, the RubMBs were re-dispersed in 12 mL ultrapure water.

The porous palladium nanospheres (pPdNSs) were prepared by a simple and effective wet-chemical method reported before.[30] Firstly, 400 μL potassium tetrachloropalladate(II) (K_2PdCl_4, 10 mM) solution and 18 mg hexadecyl pyridinium chloride (HDPC) were dissolved into 5 mL ultrapure water. After adequate mixing, 300 μL freshly prepared L-ascorbic acid (AA, 0.1 M) solution was rapidly added into the above mixture under gentle agitation. Afterwards, the resultant solution was allowed to stand for 3 h at 35 ºC. Following that, the products were obtained by centrifugation and washed using ultrapure water. Finally, the resultants were dispersed in 20 mL ultrapure water for further use.

2.3 Preparation of triplex-DNA/Au@Fe_3O_4 composites

Primarily, the mixture of thiol-labeled S0 (S0-SH, 10 μM, activated by 2 μL of 10 mM tris-(2-carboxethyl)-phosphine hydrochloride (TCEP) for 1 h to reduce disulfide bonds[31] of the S0-SH), digoxigenin-labeled S1 (S1-Dig, 10 μM), digoxigenin-labeled S2

(S2-Dig, 10 μM) and cargo DNA (substitute target, 12 μM) solution was heated to 95 ºC for 5 min, followed by gradually cooling down to room temperature to form the triplex-DNA nanomachine. Then the obtained triplex-DNA nanomachine solution was added into the suspension of Au@Fe_3O_4 and incubated overnight at 37 ºC to form triplex-DNA/Au@Fe_3O_4 composites. Eventually, the obtained triplex-DNA/Au@Fe_3O_4 composites solution was stored at 4 ºC for future use.

2.4 Fabrication of the ECL biosensor

To obtain the clean and smooth surface of glass carbon electrode (GCE, Φ = 4 mm), the bare GCE was treated based on the published method.[32] Then, 10 μL the as-prepared RubMBs solution was coated on the pre-treated GCE to obtain the RubMBs-modified electrode (RubMBs/GCE). After drying, 8 μL the pPdNSs solution was dropped onto the surface RubMBs/GCE and dried at 25 ºC, which was successfully assembled on RubMBs through electrostatic interaction. Subsequently, 10 μL S4-S5 duplex DNA solution, which was prepared by the annealing of the thiol-labeled S4 (S4-SH, 3 mM, treated with TCEP) and ferrocene-modified S5 (S5-Fc, 3 μM), was immobilized on the modified electrode (pPdNSs/RubMBs/GCE) overnight at 4 ºC *via* Pd-S bond. After rinsing with ultrapure water, 10 μL hexanethiol (HT, 1 mM) was dropped on the surface of the above electrode and incubated at room temperature for 40 min to obtain the biosensor (HT/S4-S5/pPdNSs/RubMBs/GCE). Prior to measurement, the obtained biosensor was rinsed with ultrapure water.

2.5 Measurement procedure

After collection by magnetic separation, the triplex-DNA/Au@Fe_3O_4 composites were re-dispersed in 100 μL target anti-Dig with various concentrations to react at 37 ºC for 45 min. In the meantime, target anti-Dig reacted with the triplex-DNA/Au@Fe_3O_4 composites by specific binding to the recognition sites of Dig which were labeled on the S1 and S2 respectively, to make the triplex-DNA open, resulting in the release of substitute target. Eventually, the resultant solution containing substitute target was collected through magnetic separation.

Next, the reaction solution was prepared by mixing 89 μL the above solution, 10 μL 10 × NEBuffer 4 and 1 μL 10000 U/mL T7 Exonuclease (T7 Exo). Then 10 μL the reaction solution was incubated on surface of the as-prepared biosensor (HT/S4-S5/pPdNSs/RubMBs/GCE) at 25 ºC for 2.5 hour, proceeding enzyme-assisted cycling strand displacement reaction (CSDR). Ultimately, ECL signal of the biosensor was recorded in 3 mL phosphate-buffered saline (PBS, 100 mM, pH 7.4) on a MPI-E electrochemiluminescence analytical system, and the working potential varied from -1 V~1.2 V at a scan rate of 0.3 V/s (PMT high-voltage 800 V, magnitude 3).

2.6 Native PAGE experiments

First, 10 μL each DNA sample was mixed with 2 μL loading buffer, and then the mixture was loaded into the prepared polyacrylamide gel (16%) for native polyacrylamide gel electrophoresis (PAGE), which was executed on a BG-verMIDI

standard vertical electrophoresis apparatus, using 1 × TBE buffer at pH 8.0 and at 100 V for 1 h 30 min. After the electrophoresis was finished, the gel was stained by GenGreen on shaker for 40 min, followed by being scanned by the Bio-Rad Gel Doc XR+ System. The results were shown in Figure S2 (Supporting Information).

3. Results and discussions

3.1 Morphology characterization of different nanomaterials

Typical electron microscopy images of different nanomaterials are displayed in Figure 1. It is clearly shown in Figure 1A that the RubMBs had the uniform block-like structure with a length of 2±1 μm and width of ~ 500 nm. The SEM image of the prepared pPdNSs is shown in Figure 1B. As presented, the monodisperse pPdNSs had a rough spherical appearance with a diameter of approximately 50±20 nm. The structure of the rough pPdNSs was further examined by transmission electron microscope (TEM) image (Figure 1C). It can be observed, the pPdNSs were chiseled porous nanostructures with tiny pore channels, which provides direct evidence for large specific areas and highly catalytic activity. Figure 1D displays the SEM image of the pPdNSs/RubMBs materials, exhibiting that the pPdNSs attached on the surface of RubMBs.

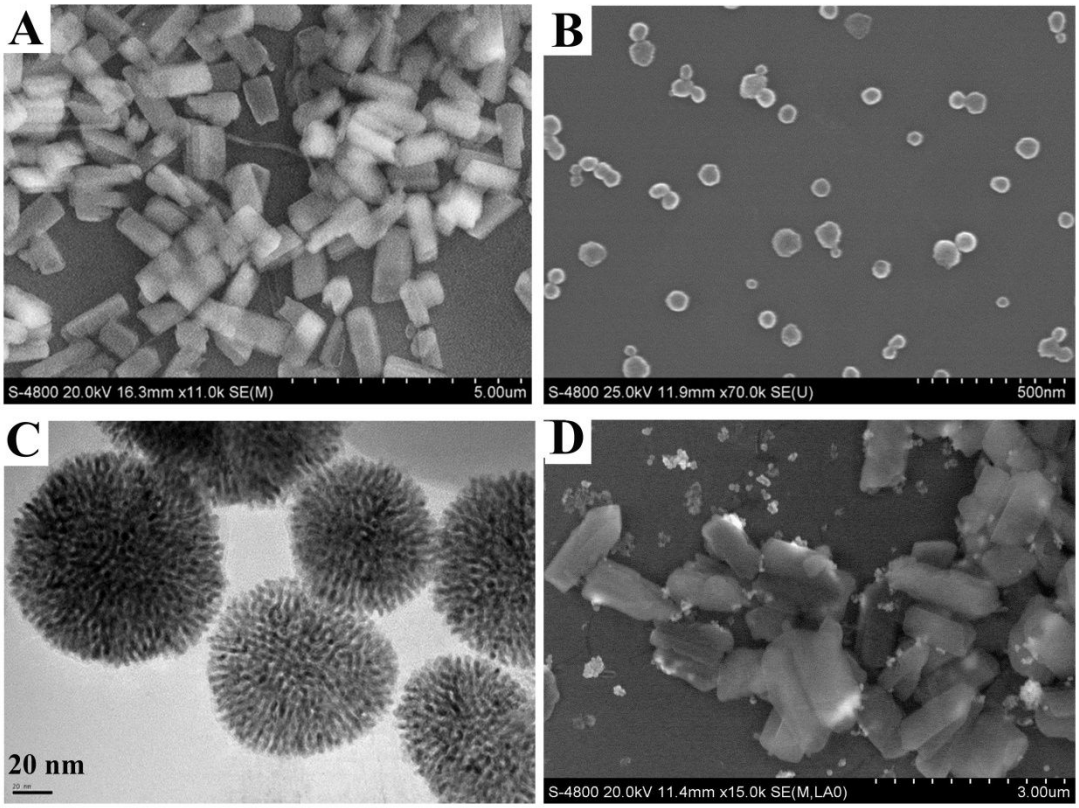

Figure 1. (A) SEM image of RubMBs, (B) SEM image of pPdNSs, (C) TEM image of pPdNSs, (D) SEM image of pPdNSs/RubMBs.

3.2 Optical characteristics of rubrene

The UV-vis absorption spectra, fluorescence spectra and ECL spectra were utilized to characterize the optical properties of rubrene THF solution and RubMBs. Figure 2A displays the normalized UV-vis absorption spectra of the rubrene in THF and the as-synthesized RubMBs in ultrapure water. Evidently, compared with rubrene in THF, the absorption peaks of RubMBs exhibits a certain red-shift from 462 nm, 491 nm, 526 nm to 470 nm, 506 nm, 592 nm, respectively, which probably results from the formation of aggregates in the J type stacking model[33,34] and the solvent effects. As observed in

Figure 2B, the fluorescence (FL) spectrum of RubMBs shows the maximum wavelength at 558 nm, which is extremely approximate to the ECL spectrum with the maximum wavelength at 550 nm, suggesting that the ECL mechanism of RubMBs might be in accord with that of photoluminescence. Additionally, the inset of Figure 2B exhibits the photographs of the RubMBs aqueous solution with the radiation of natural-light and UV-light. It can be observed that the RubMBs solution is pink-orange under natural-light but is faintly greenish yellow under the UV-light (λ = 365 nm).

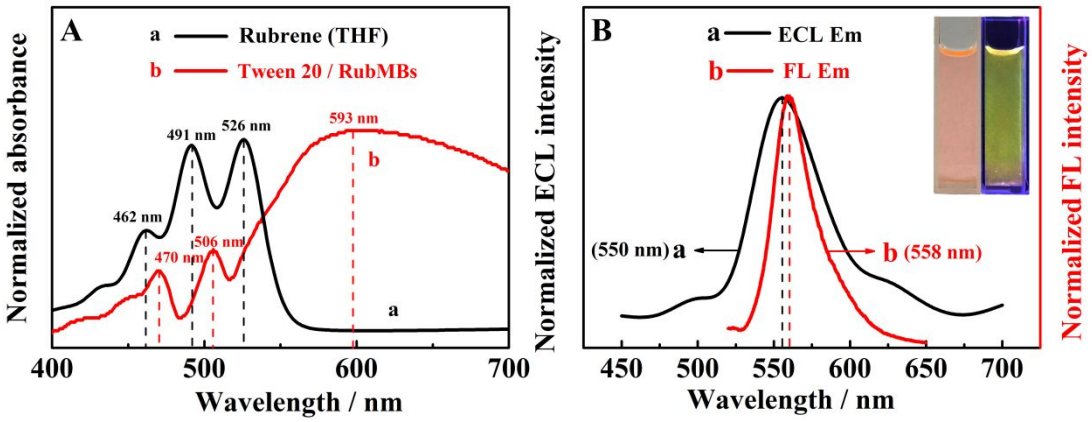

Figure 2. (A) UV-vis absorption spectra of (a) rubrene in tetrahydrofuran (THF), (b) RubMBs in ultrapure water, (B) The ECL spectrum of (a) RubMBs and FL spectrum of (b) RubMBs with the excitation wavelength at 488 nm. Inset of B: images of RubMBs with the radiation of natural-light (left) and UV-light (right).

3.3 The comparison of different co-reaction accelerators

To discuss the catalytic effect of pPdNSs and PtNFs as co-reaction accelerator for RubMBs/dissolved O_2 ECL system, a comparison test was carried out. Firstly, the Pt nanoflowers (PtNFs) were synthesized based on the reported method.[35] It is worth noting

that the initial concentration of the dihydrogen hexachloroplatinate (H_2PtCl_6) is equal to that of K_2PdCl_4 (10 mM), and then the obtained PtNFs was re-dispersed in 20 mL ultrapure water, which was the same as the treatment of pPdNSs. Subsequently, the two different modified electrodes (pPdNSs/RubMBs/GCE, PtNFs/RubMBs/GCE) were constructed according to the above mentioned method (Experimental methods 2.4), and then measured in 3 mL PBS (100 mM, pH 7.4), respectively. As shown in Figure 3A, the ECL signal of the RubMBs/dissolved O_2/pPdNSs system is 14624 a.u., which is about 3 times as much as that of RubMBs/dissolved O_2/PtNFs system (Figure 3B, 4837 a.u.), illustrating that the pPdNSs have more excellent catalytic effect and higher catalytic efficiency than PtNFs for the RubMBs/dissolved O_2 ECL system.

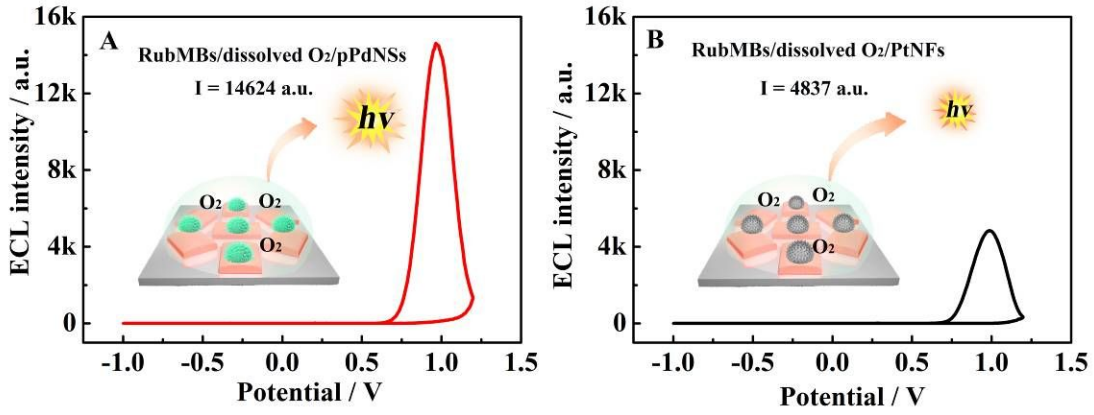

Figure 3. ECL intensity-potential curves of (A) pPdNSs/RubMBs/GCE (10 μL RubMBs solution, 10 μL pPdNSs solution), (B) PtNFs/RubMBs/GCE (10 μL RubMBs solution, 10 μL PtNFs solution) in 3 mL PBS (pH 7.4).

3.4 Possible ECL mechanism of the proposed ternary ECL system

To discuss possible ECL mechanism of the proposed ternary ECL system

(RubMBs/dissolved O_2/pPdNSs), the ECL and CV measurements of the different nanomaterial modified electrode were conducted in air-saturated and N_2-saturated PBS (pH 7.4) under the scan potential range of -1 to 1.2 V, respectively. As shown in the Figure 4A, the RubMBs/GCE shows an extremely feeble ECL signal about 41 a.u. in N_2-saturated PBS (curve a), which presents no apparent change compared with that of the pPdNSs/RubMBs/GCE (curve b). These results suggest that the pPdNSs have no effect on the ECL of RubMBs. While the RubMBs/GCE measured in air-saturated PBS presents a noticeable ECL peak with the intensity of 290 a.u. (curve c), illustrating that the dissolved O_2 can be served as the co-reactant of RubMBs to increase its ECL emission. This provides a direct evidence for the luminescence of RubMBs/dissolved O_2 ECL system. After the pPdNSs are introduced into RubMBs/dissolved O_2 ECL system, the ECL intensity is raised from 290 a.u. to 9216 a.u. (around 30 times increase, curve d), illustrating that the pPdNSs as the co-reaction accelerator can enormously improve the ECL emission of RubMBs/dissolved O_2 system.

Meanwhile, the corresponding CV curves are presented in Figure 4B. For the RubMBs/GCE measured in N_2-saturated PBS, no redox peak is observed on curve a while on the CV curve of pPdNSs/RubMBs/GCE, an anodic peak appeared at ~0 V (curve b), which may be derived from the oxidation of pPdNSs. Additionally, the current of curve b markedly increases, suggesting that the pPdNSs can improve the conductivity of the RubMBs/GCE. Remarkably, the CV wave of RubMBs/GCE in air-saturated PBS

shows a distinct cathodic peak at -0.69 V with low current (curve c), which results from the electrocatalytic reduction of dissolved O_2 in PBS. Interestingly, after the pPdNSs are introduced into the RubMBs/GCE, the corresponding cathodic peak current further increases, and the peak potential shifts positively from -0.69 V to -0.55 V (curve d), demonstrating that the pPdNSs as the co-reaction accelerator can catalyze the reduction of dissolved O_2.

Hence, based on the above discussion and the reported literature,[36-38] the possible ECL mechanism of RubMBs/dissolved O_2/pPdNSs ECL system can be outlined as follows: First, the radical cation of rubrene ($Rub^{\bullet+}$) is generated by one-electron oxidation of the RubMBs (eq 1). Then, with the aid of pPdNSs, the dissolved O_2 accumulated in perpendicular pore channels of pPdNSs is reduced to produce more ROS (eq 2-5). Subsequently, the radical cation of rubrene interacts with the ROS to generate the excited-state species ($^1R^*$) by chemical excitation (eq 6-7). Eventually, the $^1R^*$ further produces the intense ECL emission (eq 8).

$$Rub - e^- \longrightarrow Rub^{\bullet+} \quad (1)$$

$$O_2 + e^- \xrightarrow{pPdNSs} O_2^{\bullet-} \quad (2)$$

$$O_2^{\bullet-} + 2H_2O + 2e^- \xrightarrow{pPdNSs} \bullet OH + 3OH^- \quad (3)$$

$$O_2 + 2H_2O + 2e^- \xrightarrow{pPdNSs} H_2O_2 + 2OH^- \quad (4)$$

$$H_2O_2 + e^- \xrightarrow{pPdNSs} OH^- + \bullet OH + O_2 \quad (5)$$

$$O_2^{\bullet-} + Rub^{\bullet+} \longrightarrow {}^1R^* + O_2 \quad (6)$$

$$\bullet OH + Rub^{\bullet +} \longrightarrow {}^{1}R^{*} + H^{+} \quad (7)$$

$${}^{1}R^{*} \longrightarrow R + h\nu \quad (8)$$

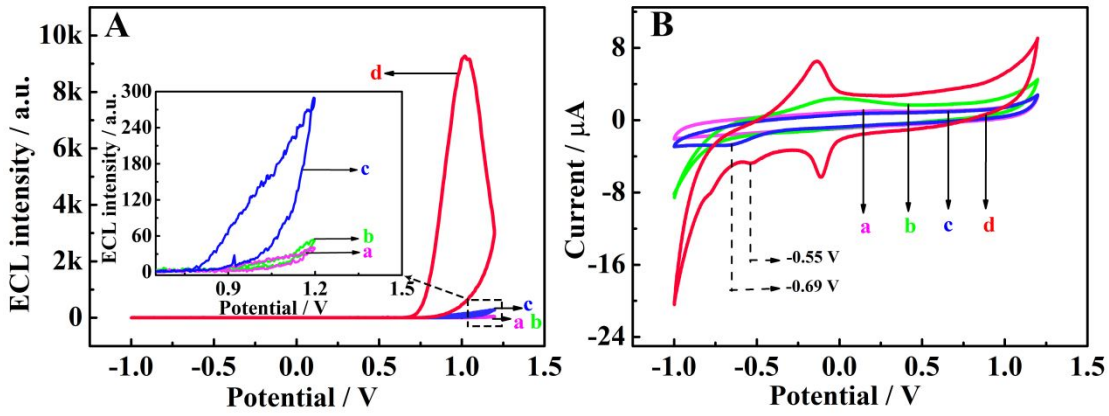

Figure 4. (A) ECL intensity-time curves and (B) the corresponding CV curves of (a) RubMBs/GCE, (b) pPdNSs/RubMBs/GCE in N_2-saturated PBS (pH 7.4), (c) RubMBs/GCE, (d) pPdNSs/RubMBs/GCE in air -saturated PBS (pH 7.4).

3.5 Optimization of the reaction conditions

With the purpose of achieving the best performance of as-prepared ECL biosensor, it is necessary for some experimental conditions to be optimized in this study, such as the reaction time of CSDR and the reaction time between triplex-DNA/Au@Fe_3O_4 composites and anti-Dig, both of which may affect ECL response of the proposed biosensor. At first, effect of the reaction time of CSDR was investigated. As demonstrated in Figure 5A, the ECL intensity keeps an upward tendency with the reaction time increasing and then basically remained stable after 2.5 h. Thus, the optimal time is served as 2.5 h used in subsequent experiment. On the other hand, the reaction time between triplex-DNA/Au@Fe_3O_4 composites and anti-Dig was studied. It is

obviously observed in Figure 5B that the ECL signal gradually tends to be stable at 45 min. Therefore, the optimal reaction time between anti-Dig and triplex-DNA/Au@Fe_3O_4 composites is determined as 45 min.

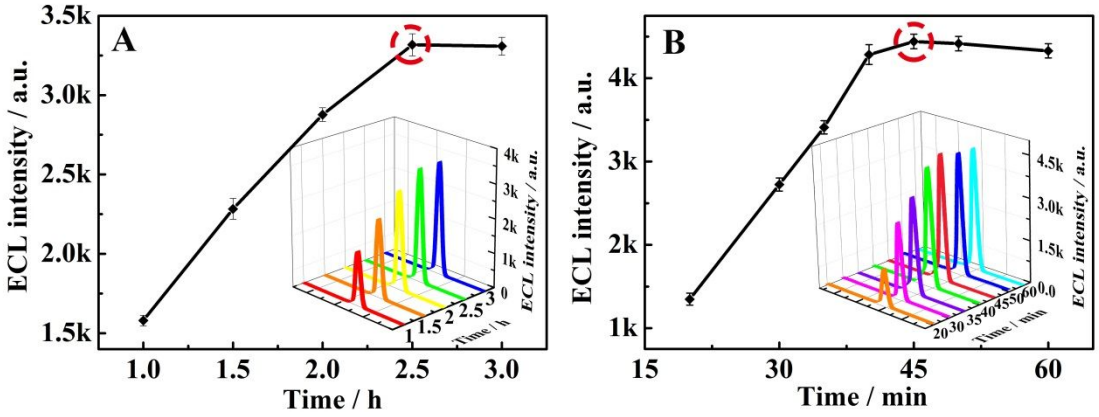

Figure 5. Effects of (A) the reaction time of CSDR, and (B) the reaction time between triplex-DNA/Au@Fe_3O_4 composites and anti-Dig (10 nM).

3.6 ECL responses of the biosensor towards anti-Dig

To investigate performance of the proposed ECL biosensor, the ECL responses to anti-Dig with various concentrations were recorded under the optimal conditions. Figure 6A displays the ECL intensity-potential curves, wherein the ECL response enhances gradually along with increasing concentration of anti-Dig ranging from 0.01 nM to 200 nM. Moreover, it can be observed from the Figure 6B that the ECL intensity (I_{ECL}) linearly depends on the logarithmic value of the anti-Dig concentration (lg$c$). And the liner relationship of the calibration plot is expressed as I_{ECL} = 13514.19 + 1120.35 lg$c$ with a squared correlation coefficient of 0.997. Satisfactorily, there is a detection limit of 6.7 pM (S/N = 3) (the detail calculation is displayed in Supporting Information Figure

S4). Additionally, compared with that reported in the previous literature, the proposed sensor exhibits outstanding analytical performance for anti-Dig detection. And the assay results are generalized in Table 1.

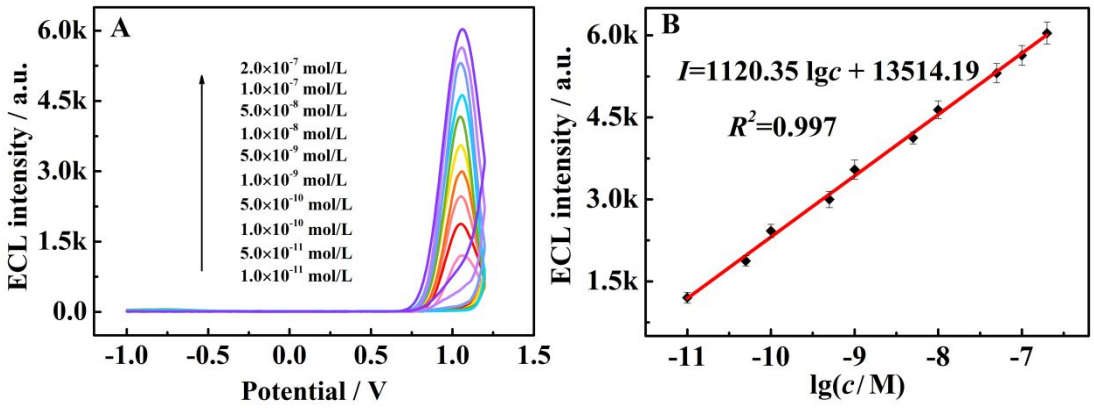

Figure 6. (A) ECL intensity-potential curves of the proposed biosensor incubated with different concentration of target anti-Dig (0.01-200 nM), (B) The calibrating plot of the proposed biosensor for anti-Dig assay. (Error bars, SD, n = 3).

Table 1. Comparison of different methods for anti-Dig detection

detection method	liner range	limit of detection	reference
Electrochemistry	none	1 nM	10
Electrochemistry	none	5 nM	39
Fluorescence	1-25 nM	0.67 nM	40
Fluorescence	10-125 nM	5.6 nM	41
Electrochemiluminescence	0.01-200 nM	6.7 pM	This work

3.7 Selectivity and stability of the biosensor

Selectivity is one of the major parameters to assess the practicability and specificity of the proposed ECL biosensor. Some relevant interfering proteins including streptavidin (STV), human immunoglobulin G (IgG) and anti-dinitrophenol (anti-DNP) at an identical

concentration of 100 nM were selected to carry out the comparative experiments. The experiment results are depicted in Figure 7A. Despite the existence of interfering proteins with high concentration, no significant effect for ECL signal is observed compared to the ECL intensity of blank sample. However, the existence of anti-Dig makes the ECL intensity significant improvement. The results obviously illustrate that the proposed ECL strategy for anti-Dig detection has an excellent selectivity and may be apply for practical analysis.

Equally, stability is also a significant concern for exploring the availability of ECL sensor, which was studied by means of periodically scanning the as-prepared sensor in 100 mM PBS (pH 7.4). The consequences are displayed in Figure 7B, It can be found that the ECL intensity of sensor basically remains stable within 10 times in the presence of 10 nM of anti-Dig (RSD = 1.14%), suggesting the proposed biosensor possesses satisfactory stability.

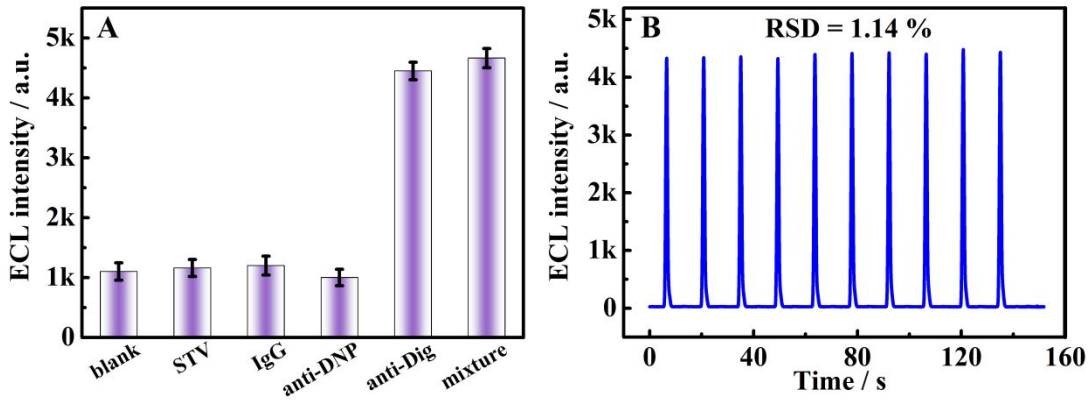

Figure 7. (A) Selectivity of the ECL biosensor for some relevant interfering proteins, (B) Stability of the ECL biosensor under a continuous scan for 10 cycles in the presence of anti-Dig (10 nM).

3.8 Analysis of anti-Dig in human serum

The feasibility and accuracy of the proposed method was evaluated by measuring the recovery of anti-Dig with known concentrations in human serum (diluted with PBS, pH 7.4). As shown in Table 2, the recovery and relative standard deviations (RSD) of anti-Dig are in the range of 90-108% and 1.0-4.0%, respectively. On the basis of the above assay results, it proves that the proposed biosensor is a potential tool for the admeasurement of anti-Dig in real samples.

Table 2. Recovery of anti-Dig in diluted human serum

Sample number	Added/nM	Detected/nM	Recovery/%	RSD/%
1	0.1	0.108	108	3.1
2	1	0.962	96.2	3.0
3	10	10.5	105	1.0
4	100	94.7	94.7	1.5
5	150	154	103	3.7

4. Conclusions

To sum up, a highly sensitive ternary ECL system (RubMBs/dissolved O_2/pPdNSs) for anti-Dig detection is established by means of uniting the advantages of the pPdNSs and triplex-DNA nanomachine in this work. First, the pPdNSs with large specific surface area can immobilize great quantities of quenching probe (S4-S5-Fc) *via* Pd-S coordinate bond. Herein, the pPdNSs as co-reaction accelerator present perfect catalytic capacity for dissolved O_2, which can enormously enhance ECL intensity and improve sensitivity of the proposed method for antibody detection. More significantly, the anti-Dig powered

triplex-DNA nanomachine in the presence of anti-Dig achieves the rapid release of cargo DNA for target amplification, which is beneficial to improving the accuracy and sensitivity of anti-Dig assay. Therefore, the proposed ECL strategy can measure anti-Dig in human serum and exhibit high accuracy and sensitivity, illustrating its high practical application value. Besides, the triplex-DNA nanomachine can be designed to response other special inputs (e g. anti-DNP, STV), which broadens its application in the bioassay.

Supporting Information

Chemicals and materials, apparatus, SEM characterization of Au@Fe_3O_4 nanocomposites, ECL and CV characterization of the ECL biosensor, feasibility analysis by native PAGE experiments, and the calculation procedure of the LOD.

Acknowledgments

This work was financially supported by the NNSF of China (21675130, 21775124, 21675129), the Natural Science Foundation Project of CQ CSTC (cstc2018jcyjAX0546) and the Fundamental Research Funds for the Central Universities (XDJK2018AA003), China.

References

(1) Janssen, B. M. G.; Lempens, E. H. M.; Olijve, L. L. C.; Voets, I. K.; van Dongen, J. L. J.; de Greef, T. F. A.; Merkx, M. Reversible Blocking of Antibodies Using Bivalent Peptide-DNA Conjugates Allows Protease-Activatable Targeting. *Chem. Sci.* **2013,** *4* (4), 1442.

(2) Tsai, C. T.; Robinson, P. V.; Spencer, C. A.; Bertozzi, C. R. Ultrasensitive Antibody Detection by Agglutination-PCR (ADAP). *ACS Cent. Sci.* **2016,** *2* (3), 139-147.

(3) Zhu, C.; Wen, Y.; Li, D.; Wang, L.; Song, S.; Fan, C.; Willner, I. Inhibition of the In Vitro Replication of DNA by an Aptamer-Protein Complex in an Autonomous DNA Machine. *Chem. Eur. J.* **2009,** *15* (44), 11898-11903.

(4) Shen, J.; Li, Y.; Gu, H.; Xia, F.; Zuo, X. Recent Development of Sandwich Assay Based on the Nanobiotechnologies for Proteins, Nucleic acids, Small molecules, and Ions. *Chem. Rev.* **2014,** *114* (15), 7631-7677.

(5) Zhang, C.; Cui, H.; Han, Y.; Yu, F.; Shi, X. Development of a Biomimetic Enzyme-Linked Immunosorbent Assay Based on Molecularly Imprinted Polymers on Paper for the Detection of Carbaryl. *Food Chem.* **2018,** *240*, 893-897.

(6) Towbin, H.; Staehelin, T.; Gordon, J. Electrophoretic Transfer of Proteins from Polyacrylamide Gels to Nitrocellulose Sheets: Procedure and Some Applications. *Proc. Natl. Acad. Sci. U. S. A.* **1979,** *76* (9), 4350-4354.

(7) White, R. J.; Kallewaard, H. M.; Hsieh, W.; Patterson, A. S.; Kasehagen, J. B.; Cash, K. J.; Uzawa, T.; Soh, H. T.; Plaxco, K. W. Wash-free, Electrochemical Platform for the Quantitative, Multiplexed Detection of Specific Antibodies. *Anal. Chem.* **2012,** *84* (2), 1098-1103.

(8) Porchetta, A.; Ippodrino, R.; Marini, B.; Caruso, A.; Caccuri, F.; Ricci, F. Programmable Nucleic Acid Nanoswitches for the Rapid, Single-Step Detection of

Antibodies in Bodily Fluids. *J. Am. Chem. Soc.* **2018,** *140* (3), 947-953.

(9) Mahshid, S. S.; Camire, S.; Ricci, F.; Vallee-Belisle, A. A Highly Selective Electrochemical DNA-Based Sensor That Employs Steric Hindrance Effects to Detect Proteins Directly in Whole Blood. *J. Am. Chem. Soc.* **2015,** *137* (50), 15596-15599.

(10) Vallee-Belisle, A.; Ricci, F.; Uzawa, T.; Xia, F.; Plaxco, K. W. Bioelectrochemical Switches for the Quantitative Detection of Antibodies Directly in Whole Blood. *J. Am. Chem. Soc.* **2012,** *134* (37), 15197-15200.

(11) Zhang, Z.; Hejesen, C.; Kjelstrup, M. B.; Birkedal, V.; Gothelf, K. V. A DNA-Mediated Homogeneous Binding Assay for Proteins and Small Molecules. *J. Am. Chem. Soc.* **2014,** *136* (31), 11115-11120.

(12) Zhu, J.; Gan, H.; Wu, J.; Ju, H. Molecular Machine Powered Surface Programmatic Chain Reaction for Highly Sensitive Electrochemical Detection of Protein. *Anal. Chem.* **2018,** *90* (8), 5503-5508.

(13) Yang, J.; Dou, B.; Yuan, R.; Xiang, Y. Aptamer/Protein Proximity Binding-Triggered Molecular Machine for Amplified Electrochemical Sensing of Thrombin. *Anal. Chem.* **2017,** *89* (9), 5138-5143.

(14) Yang, Z. H.; Zhuo, Y.; Yuan, R.; Chai, Y. Q. Highly Effective Protein Converting Strategy for Ultrasensitive Electrochemical Assay of Cystatin C. *Anal. Chem.* **2016,** *88* (10), 5189-5196.

(15) Li, L.; Chen, Y.; Zhu, J. J. Recent Advances in Electrochemiluminescence Analysis.

Anal. Chem. **2017,** *89* (1), 358-371.

(16) Zhang, P.; Jiang, J.; Yuan, R.; Zhuo, Y.; Chai, Y. Highly Ordered and Field-Free 3D DNA Nanostructure: The Next Generation of DNA Nanomachine for Rapid Single-Step Sensing. *J. Am. Chem. Soc.* **2018,** *140* (30), 9361-9364.

(17) Feng, Y.; Sun, F.; Wang, N.; Lei, J.; Ju, H. Ru $(bpy)_3^{2+}$ Incorporated Luminescent Polymer Dots: Double-Enhanced Electrochemiluminescence for Detection of Single-Nucleotide Polymorphism. *Anal. chem.* **2017,** *89* (14), 7659-7666.

(18) Zhang, Y.; Yang, H.; Cui, K.; Zhang, L.; Xu, J.; Liu, H.; Yu, J. Highly Conductive and Bendable Gold Networks Attached on Intertwined Cellulose Fibers for Output Controllable Power Paper. *J. Mater. Chem. A.* **2018,** DOI: 10.1039/C8TA08293F.

(19) Zhang, Y.; Wang, L.; Luo, F.; Qiu, B.; Guo, L.; Weng, Z.; Lin, Z.; Chen, G. An Electrochemiluminescence Biosensor for Kras Mutations Based on Locked Nucleic Acid Functionalized DNA Walkers and Hyperbranched Rolling Circle Amplification. *Chem. Commun.* **2017,** *53* (20), 2910-2913.

(20) Bezman, R.; Faulkner, L. R. Mechanisms of Chemiluminescent Electron-Transfer Reactions. V. Absolute Measurements of Rubrene Luminescence in Benzonitrile and N, N-Dimethylformamide. *J. Am. Chem. Soc.* **1972,** *94* (18), 6324-6330.

(21) Liu, J. L.; Tang, Z. L.; Zhang, J. Q.; Chai, Y. Q.; Zhuo, Y.; Yuan, R. Morphology-Controlled 9,10-Diphenylanthracene Nanoblocks as Electrochemiluminescence Emitters for MicroRNA Detection with One-Step DNA

Walker Amplification. *Anal. Chem.* **2018,** *90* (8), 5298-5305.

(22) Li, L. L.; Li, K.; Li, M. Y.; Shi, L.; Liu, Y. H.; Zhang, H.; Pan, S. L.; Wang, N.; Zhou, Q.; Yu, X. Q. BODIPY-Based Two-Photon Fluorescent Probe for Real-Time Monitoring of Lysosomal Viscosity with Fluorescence Lifetime Imaging Microscopy. *Anal. Chem.* **2018,** *90* (9), 5873-5878.

(23) Dick, J. E.; Renault, C.; Kim, B. K.; Bard, A. J. Electrogenerated Chemiluminescence of Common Organic Luminophores in Water Using an Emulsion System. *J. Am. Chem. Soc.* **2014,** *136* (39), 13546-13549.

(24) Liu, J. L.; Tang, Z. L.; Zhuo, Y.; Chai, Y. Q.; Yuan, R. Ternary Electrochemiluminescence System Based on Rubrene Microrods as Luminophore and Pt Nanomaterials as Coreaction Accelerator for Ultrasensitive Detection of MicroRNA from Cancer Cells. *Anal. Chem.* **2017,** *89* (17), 9108-9115.

(25) Ranallo, S.; Prevost-Tremblay, C.; Idili, A.; Vallee-Belisle, A.; Ricci, F. Antibody-Powered Nucleic Acid Release Using a DNA-Based Nanomachine. *Nat. Commun.* **2017,** *8*, 15150.

(26) Ranallo, S.; Rossetti, M.; Plaxco, K. W.; Vallee-Belisle, A.; Ricci, F. A Modular, DNA-Based Beacon for Single-Step Fluorescence Detection of Antibodies and Other Proteins. *Angew. Chem. Int. Ed.* **2015,** *54* (45), 13214-13218.

(27) Zhao, J.; Liang, W. B.; Lei, Y. M.; Ou, Y. X.; Chai, Y. Q.; Yuan, R.; Zhuo, Y. An Efficient Electrochemiluminescence Amplification Strategy *via* Bis-co-reaction

Accelerator for Sensitive Detection of Laminin to Monitor Overnutrition Associated Liver Damage. *Biosens. Bioelectron.* **2017,** *98*, 317-324.

(28) Zhou, Y.; Chen, M.; Zhuo, Y.; Chai, Y.; Xu, W.; Yuan, R. In Situ Electrodeposited Synthesis of Electrochemiluminescent Ag Nanoclusters as Signal Probe for Ultrasensitive Detection of Cyclin-D1 from Cancer Cells. *Anal. Chem.* **2017,** *89* (12), 6787-6793.

(29) Zhang, P.; Lin, Z.; Zhuo, Y.; Yuan, R.; Chai, Y. Dual microRNAs-Fueled DNA Nanogears: A Case of Regenerated Strategy for Multiple Electrochemiluminescence Detection of microRNAs with Single Luminophore. *Anal. Chem.* **2017,** *89* (2), 1338-1345.

(30) Huang, X.; Li, Y.; Chen, Y.; Zhou, E.; Xu, Y.; Zhou, H.; Duan X.; Huang, Y. Palladium-Based Nanostructures with Highly Porous Features and Perpendicular Pore Channels as Enhanced Organic Catalysts. *Angew. Chem.* **2013,** *125* (9), 2580-2584.

(31) Xu, J.; Zhang, Y.; Li, L.; Kong, Q.; Zhang, L.; Ge, S.; Yu, J. Colorimetric and Electrochemiluminescence Dual-Mode Sensing of Lead Ion Based on Integrated Lab-on-Paper Device. *ACS Appl. Mater. Interfaces* **2018,** *10* (4), 3431-3440.

(32) Wu, F. F.; Zhou, Y.; Zhang, H.; Yuan, R.; Chai, Y. Q. Electrochemiluminescence Peptide-Based Biosensor with Hetero-Nanostructures as Coreaction Accelerator for the Ultrasensitive Determination of Tryptase. *Anal. Chem.* **2018,** *90* (3), 2263-2270.

(33) Mahajan, P. G.; Bhopate, D. P.; Kamble, A. A.; Dalavi, D. K.; Kolekar, G. B.; Patil, S. R. Selective Sensing of Fe^{2+} Ions in Aqueous Solution Based on Fluorescence

Quenching of SDS Capped Rubrene Nanoparticles: Application in Pharmaceutical Formulation. *Anal. Methods* **2015,** *7* (18), 7889-7898.

(34) Kim, H. Y.; Bjorklund, T. G.; Lim, S. H.; Bardeen, C. J. Spectroscopic and Photocatalytic Properties of Organic Tetracene Nanoparticles in Aqueous Solution. *Langmuir* **2003,** *19* (9), 3941-3946.

(35) Yin, J.; Wang, J.; Li, M.; Jin, C.; Zhang, T. Iodine Ions Mediated Formation of Monomorphic Single-Crystalline Platinum Nanoflowers. *Chem. Mater.* **2012,** *24* (14), 2645-2654.

(36) Chin, D. H.; Chiericato Jr, G.; Nanni Jr, E. J.; Sawyer, D. T. Proton-Induced Disproportionation of Superoxide Ion in Aprotic Media. *J. Am. Chem. Soc.* **1982,** *104* (5), 1296-1299.

(37) Sawyer, D. T.; Valentine, J. S. How Super Is Superoxide?. *Acc. Chem. Res.* **1981,** *14* (12), 393-400.

(38) AlNashef, I. M.; Leonard, M. L.; Kittle, M. C.; Matthews, M. A.; Weidner, J. W. Electrochemical Generation of Superoxide in Room-Temperature Ionic Liquids. *Electrochem. Solid-State Lett.* **2001,** *4* (11), D16-D18.

(39) Cash, K. J.; Ricci, F.; Plaxco, K. W. An Electrochemical Sensor for the Detection of Protein-Small Molecule Interactions Directly in Serum and Other Complex Matrices. *J. Am. Chem. Soc.* **2009,** *131* (20), 6955-6957.

(40) Dou, B.; Yang, J.; Shi, K.; Yuan, R.; Xiang, Y. DNA-Mediated Strand Displacement

Facilitates Sensitive Electronic Detection of Antibodies in Human Serums. *Biosens. Bioelectron.* **2016,** *83*, 156-161.

(41) Peng, Y.; Li, X.; Yuan, R.; Xiang, Y. Steric Hindrance Inhibition of Strand Displacement for Homogeneous and Signal-on Fluorescence Detection of Human Serum Antibodies. *Chem. Commun.* **2016,** *52* (85), 12586-12589.

Table of Contents (TOC)